

DOI: 10.1002/cphc.201402351

Nonuniform Continuum Model for Solvatochromism Based on Frozen-Density Embedding Theory

Sapana Vitthal Shedge and Tomasz A. Wesolowski*^[a]

Frozen-density embedding theory (FDET) provides the formal framework for multilevel numerical simulations, such that a selected subsystem is described at the quantum mechanical level, whereas its environment is described by means of the electron density (frozen density; $\rho_B(\vec{r})$). The frozen density $\rho_B(\vec{r})$ is usually obtained from some lower-level quantum mechanical methods applied to the environment, but FDET is not limited to such choices for $\rho_B(\vec{r})$. The present work concerns the application of FDET, in which $\rho_B(\vec{r})$ is the statistically averaged electron density of the solvent $\langle \rho_B(\vec{r}) \rangle$. The specific

solute–solvent interactions are represented in a statistical manner in $\langle \rho_B(\vec{r}) \rangle$. A full self-consistent treatment of solvated chromophore, thus involves a single geometry of the chromophore in a given state and the corresponding $\langle \rho_B(\vec{r}) \rangle$. We show that the coupling between the two descriptors might be made in an approximate manner that is applicable for both absorption and emission. The proposed protocol leads to accurate (error in the range of 0.05 eV) descriptions of the solvatochromic shifts in both absorption and emission.

1. Introduction

The effect of solvent on the UV/Vis spectra of organic dyes is a topic of great interest.^[1–5] The position, shape, and intensity of electronic transition bands are affected by the interaction of the solute with solvent molecules; therefore, the bands carry indirect information about both the electronic structure of the dye as well as the structure of the solvent. Numerical modelling of the solvent effect is a well-established tool for extracting such information. Large numbers of experimental and theoretical studies are devoted to solvatochromism in organic dyes.^[6–8] Numerical simulation methods are capable of modelling accurately the solvent effects on the maxima of the absorption (and emission) bands (λ_{\max}) measured experimentally and referred to as solvatochromic shifts throughout the present work. They can be divided into “supermolecular” or embedding methods. In supermolecular simulations, the solvent is represented by means of a limited number of molecules, which are treated at the same quantum-mechanical level as the chromophore. The present work concerns the embedding strategy, in which the highest level of quantum-mechanical treatment of the excited states is used for only a chromophore (and possibly a few solvent molecules), whereas the remaining solvent is represented by means of some embedding operator. Various strategies have been developed over the last few decades to obtain the embedding operator and the corresponding energy for practical simulations (see for instance reviews

given in Refs. [7,9–13]). Such operators are known under various names, reflecting their basic features (hybrid methods, QM/MM, QM/MD, QM/QM', FDE, PCM, COSMO, ONIOM, just to name a few examples). Each of them can be used within a simplified single-geometry picture of the solvated chromophore or in a more complete statistical representation taking into account fluctuations of the geometry or even conformational changes. The representation of the solvent in the embedding methods can be either explicit (atomistic resolution) or implicit (continuum models). Most commonly used continuum models of the solvent such as polarizable uniform continuum model (PCM)^[14] or COSMO^[15,16] do not take into account specific solvent–solute interactions. In the reference interaction site model (RISM),^[17] the continuum level of description for the solvent is retained but the specific interactions are taken into account implicitly. RISM-type models were originally introduced to study structure and thermodynamics of classical liquids. Teno, Hirata, and Kato introduced a self-consistent hybrid RISM approach to also study the effect of solvents on the electronic structure of the solute molecules.^[18] They combined ab initio Hartree–Fock method with RISM integral equation theory. Kovalenko and Hirata^[19,20] formulated a self-consistent combination of 3D-RISM with Kohn–Sham density functional theory (DFT)^[21] methods. Kaminski et al.^[22] adopted the same approach to generate the average positive (nuclei) and negative (electrons) charge densities as input quantities for frozen-density embedding theory (FDET) based calculations of solvatochromic shifts in absorption. A comprehensive overview of the performance of such combination is provided in Ref. [23]. Similar to other continuum models of the solvent, the FDET/3D-RISM strategy can provide only solvatochromic shifts and not shapes of the bands. It uses a single-geometry representation of the chromophore. Neither homogeneous line-broadening due to the fluc-

[a] Dr. S. V. Shedge, Prof. T. A. Wesolowski
Université de Genève
Département de Chimie Physique 30
quai Ernest-Ansermet
CH-1211 Genève 4 (Switzerland)
E-mail: sapnavshedge@gmail.com

 Supporting Information for this article is available on the WWW under
<http://dx.doi.org/10.1002/cphc.201402351>.

tuation of the chromophore geometry nor inhomogeneous broadening due to the statistical nature of the solvent can be taken into account. The average charge densities do not carry any information about the structural fluctuations in the system. The multilevel character of the FDET/3D-RISM simulations is reflected not only in different descriptors used for the chromophore ($\rho_A(\vec{r})$) and the solvent ($\langle \rho_B(\vec{r}) \rangle$) but in different treatment of the coupling between the state of the solute and the solvent. Any change in $\langle \rho_B(\vec{r}) \rangle$ affects $\rho_A(\vec{r})$ through the effective FDET embedding potential, whereas the effect of the change in the state of the solute (electronic excitation and geometry) affects $\langle \rho_B(\vec{r}) \rangle$ through pair-potentials in 3D-RISM (see Figure 1).

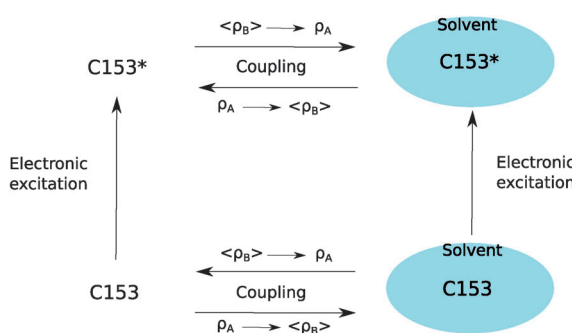


Figure 1. Single-geometry representation of the considered states of C153 and the couplings between the state-descriptors for the chromophore ($\rho_A(\vec{r})$) and the solvent ($\langle \rho_B(\vec{r}) \rangle$). In all calculations, the effect of $\langle \rho_B(\vec{r}) \rangle$ on $\rho_A(\vec{r})$ is taken into account by the FDET embedding potential. Simplified treatment of the opposite effect is considered in the present work (Models 1–3).

In our original implementation of the FDET/3D-RISM strategy, the effect of changes in ρ_A on $\langle \rho_B(\vec{r}) \rangle$ was taken into account by modifying the corresponding net atomic charges of the chromophore. Assuring the full self-consistency in this manner might lead, however, to numerically unstable algorithms due to lack of uniqueness in casting the electron density of the solute into the form of atomic point charges. The problems can be expected to be aggravated in the case of emission for two reasons: larger delocalization of electron density and possible larger solvent effect on the geometry of the chromophore in the excited state.

In the present work, we propose a simplified treatment of the influence of the changes in the state of the solvent on $\langle \rho_B(\vec{r}) \rangle$. Turning back to the issue of the coupling between the change in $\rho_A(\vec{r})$ and the resulting change of $\langle \rho_B(\vec{r}) \rangle$ it is worthwhile noting the difference between the present case and the case of an atomistic level description for the environment. In the case of an atomistic level of description for both the embedded subsystem and its environment, it is possible to take into account this coupling by means of exchanging the role of subsystems A and B in all FDET equations and optimize also the electron density $\rho_B(\vec{r})$ together with $\rho_A(\vec{r})$. For intermolecular complexes, such “freeze-and-thaw”^[24] procedure to optimize both $\rho_A(\vec{r})$ and $\rho_B(\vec{r})$ was shown to converge quickly. In the case of continuum description of the environment, coupling

the subsystems in this way is not possible because the Born–Oppenheimer density of the environment ($\rho_B(\vec{r})$) is not available. The effect of the changes in $\rho_A(\vec{r})$ on the average solvent density $\langle \rho_B(\vec{r}) \rangle$ is taken into account in the pair potentials used in the 3D-RISM equations. The change of the parameters in the potentials due to changes in $\rho_A(\vec{r})$ leads to the change in the nuclear site probabilities, which are subsequently dressed up with the same electronic cloud for each type of atom in the solvent. This might suggest that changes in the electronic polarization of the environment are not taken into account. The issue of accounting for electronic polarization in $\rho_B(\vec{r})$ is not straightforward in FDET, because of the admissible situation that the same total density is obtained for different choices for $\rho_B(\vec{r})$. This manifests itself in a rather weak dependence of the numerical results on the choice for $\rho_B(\vec{r})$ ^[25] and reflects the variational principle basis of FDET. The attribution of the change of the excitation energies, which result from the optimization of $\rho_B(\vec{r})$, only to the electronic polarization of the environment as previously reported (see a recent publication by Daday et al.,^[26] in which the FDET embedding potential was used to obtain excited states of a system described by means of embedded interacting wave function, or our own work on embedded trivalent cation in highly polarizable environment)^[27] has only qualitative value. The effect due to the polarization of the electron density of the environment on the properties of the embedded species cannot be separated from the effect due to the error in the used approximation for the non-additive kinetic potential.

The proposed method for modeling solvatochromic shifts in both absorption and emission is applied for coumarin 153 (C153) in several solvents of different polarity ranging from cyclohexane to water. C153 is a well-studied laser probe with characterized low-lying $\pi \rightarrow \pi^*$ excitation.^[6,28] It shows high solvatochromic and Stokes shifts, due to pronounced change in dipole moment and geometry upon excitation. Previously, we have studied solvatochromic shifts in the absorption band of C153 by using FDET/3D-RISM,^[23] however, the present study focuses on testing our key approximations on the same model for simulation of solvatochromic shifts in the emission band.

2. Theoretical Details

2.1. Frozen-Density Embedding Theory

FDET^[29–32] concerns minimizing the total energy for a system comprising N electrons in the external potential $v(\vec{r})$ in the presence of the constraint $\rho(\vec{r}) \geq \rho_B(\vec{r})$ all over the \mathbf{R}^3 space [Eq. (1)]:

$$E_{\text{emb}}[\rho_B] = \min_{\rho \geq \rho_B \geq 0} E_v^{\text{HK}}[\rho] \quad (1)$$

$$\int \rho(\vec{r}) d\vec{r} = N$$

where $E_v^{\text{HK}}[\rho]$ is the Hohenberg–Kohn functional of the total energy^[33] and ρ_B is a given function. For the sake of application of FDET in multilevel numerical simulations, in which the state

of a selected part of a larger system is described by using explicit quantum mechanical descriptors and the state of the remaining part is described by using only electron density, we refer to ρ_B as frozen density. For the same reasons, we split the total external potential $v(\vec{r})$ into two parts ($v(\vec{r}) = v_A(\vec{r}) + v_B(\vec{r})$), where $v_B(\vec{r})$ is the external potential generated by (usually nuclei) of the environment. There are no other constraints for $\rho_B(\vec{r})$ than those given in Equation (1). The energy $E_{\text{emb}}[\rho_B]$ is, by construction, the upper bound of the ground-state energy of the whole system. In FDET, $E_{\text{emb}}[\rho_B]$ is obtained from Euler–Lagrange equations for the energy functional, which depends on both the quantum mechanical descriptor for the embedded system and the given frozen density $\rho_B(\vec{r})$. In the case of interacting wavefunction, Ψ^A is used as the quantum descriptor; this functional is given in Equation (2):

$$\begin{aligned} E_{AB}^{\text{EWF}}[\Psi^A, \rho_B] = & \langle \Psi^A | \hat{H}_A | \Psi^A \rangle + \Delta E^{\text{MD}}[\rho_A] + E_{v_B}^{\text{HK}}[\rho_B] + \\ & + \int \rho_A(\vec{r}) v_B(\vec{r}) d\vec{r} + \int \int \frac{\rho_A(\vec{r}) \rho_B(\vec{r}')}{|\vec{r} - \vec{r}'|} d\vec{r} d\vec{r}' \\ & + T_s^{\text{nad}}[\rho_A, \rho_B] + E_{xc}^{\text{nad}}[\rho_A, \rho_B] \\ & + \int \rho_B(\vec{r}) v_A(\vec{r}) d\vec{r} \end{aligned} \quad (2)$$

where: 1) ρ_A denotes the electron density corresponding to Ψ^A ; 2) $X^{\text{nad}}[\rho_A, \rho_B]$ denotes the bifunctional $X^{\text{nad}}[\rho_A, \rho_B] = X[\rho_A + \rho_B] - X[\rho_A] - X[\rho_B]$ (with $X[\rho] = T_s[\rho]$ or $E_{xc}[\rho]$ being density functionals for the noninteracting reference kinetic energy and exchange-correlation energy, respectively, defined in the constrained search procedure),^[34,35] 3) the functional $\Delta E^{\text{MD}}[\rho_A]$ represents the part of the correlation energy functional that is not taken into account by a wavefunction-based method (see Ref. [31] for details), and 4) $E_{v_B}^{\text{HK}}[\rho_B]$ denotes the Hohenberg–Kohn energy functional^[33] corresponding to $v_B(\vec{r})$.

If a noninteracting reference system of electrons (Ψ_s^A) is used as quantum mechanical descriptor for the embedded system, the corresponding energy functional is described by Equation (3):

$$\begin{aligned} E_{AB}^{\text{EKS}}[\Psi_s^A, \rho_B] = & E^{\text{KS}}[\Psi_s^A] \\ & + \int \rho_A(\vec{r}) v_B(\vec{r}) d\vec{r} + \int \int \frac{\rho_A(\vec{r}) \rho_B(\vec{r}')}{|\vec{r} - \vec{r}'|} d\vec{r} d\vec{r}' \\ & + T_s^{\text{nad}}[\rho_A, \rho_B] + E_{xc}^{\text{nad}}[\rho_A, \rho_B] \\ & + \int \rho_B(\vec{r}) v_A(\vec{r}) d\vec{r} \end{aligned} \quad (3)$$

where $E_{v_A}^{\text{KS}}[\Psi_s^A]$ is a familiar expression for the energy of a Kohn–Sham system in an external potential $v_A(\vec{r})$ expressed as a functional of the Slater determinant constructed from Kohn–Sham orbitals.^[21]

A similar expression to the those given in Equations (2) and (3) for the total energy functional is given in Ref. [32] for the case of embedded one-particle reduced density matrix.

The Euler–Lagrange equation is used to optimize the quantum mechanical descriptor for the embedded system. It is given in Equation (4) for the case of noninteracting embedded wavefunction $-\Psi_s^A$:

$$\frac{\delta E_{AB}^{\text{EKS}}[\Psi_s^A, \rho_B]}{\delta \Psi_s^A} - \lambda \Psi_s^A = 0 \quad (4)$$

The procedure to solve the Euler–Lagrange equation depends on the chosen quantum mechanical descriptor and involves a modification of the working equations in the environment-free case; that is, for $v_B(\vec{r}) = 0$ and $\rho_B(\vec{r}) = 0$ by addition of the embedding potential described by Equation (5):

$$\begin{aligned} v_{\text{emb}}[\rho_A, \rho_B; \vec{r}] = & \zeta_B(\vec{r}) + \int \frac{\rho_B(\vec{r}')}{|\vec{r}' - \vec{r}|} d\vec{r}' + \frac{\delta T_s^{\text{nad}}[\rho_A, \rho_B]}{\delta \rho_A(\vec{r})} \\ & + \frac{\delta E_{xc}^{\text{nad}}[\rho_A, \rho_B]}{\delta \rho_A(\vec{r})} \end{aligned} \quad (5)$$

In the case of embedded noninteracting wavefunction (Ψ_s^A , in the case considered in the present work), the FDET embedding potential is added to the Kohn–Sham expression for the effective potential in the absence of the environment. In the case of embedded interacting wavefunction, the FDET embedding potential is added to the external potential $v_A(\vec{r})$.

The key features of the FDET embedding potential given in Equation (5) and reflected in the notation are: 1) it is local, 2) it is expressed as a functional of $\rho_B(\vec{r})$, and 3) it depends on $\rho_A(\vec{r})$. The last property results in the fact that the corresponding energy is not a simple integral of the product of the embedding potential and the density, which distinguishes the FDET embedding potential qualitatively from the electrostatic potential generated by the environment. The electrostatic potential, which is the classical component of the FDET embedding potential, is commonly used in simulations based on the embedding strategy. The use of the full FDET embedding potential in multilevel types of simulations is growing (for example, see Refs. [36–42]) especially since the pioneering work of Carter and collaborators,^[43] who combined the embedding potential introduced by Wesolowski and Warshel for embedding a noninteracting reference system with methods taking into account the electron correlations in the embedded subsystem explicitly. Such a combination has a clear interpretation in FDET in the case of the variational-principle-based wavefunction-theory methods given in Ref. [31] and outlined in the present section.

Equations (1)–(5) provide a complete formal framework of FDET leading to a self-consistent, embedded wavefunction, the upper bound of the ground-state energy of the total system, and the embedding potential. In practical applications of methods based on FDET, $\rho_B(\vec{r})$ is an input quantity that is provided by a suitable chosen method (quantum mechanical, classical, experiment, and so forth). All results are functionals of the provided $\rho_B(\vec{r})$. Moreover, the approximations for the bifunctionals $T_s^{\text{nad}}[\rho_A, \rho_B]$ and $E_{xc}^{\text{nad}}[\rho_A, \rho_B]$ affect the quality of the obtained results on top of approximations used to describe

the embedded subsystem in the absence of any environment, that is, at $v_B(\vec{r}) = 0$ and $\rho_B(\vec{r}) = 0$. If the density functional approximations are used in FDET equations, the notion of the upper bound does not refer to an exact value of the total energy but to the energy obtained with a complete basis set for a given approximation of the density functionals. The situation is similar in the density functional theory formulation of the many-electron quantum problem.

The generalization of the above framework for excited states is especially simple within the linear-response time-dependent DFT framework (LR-TDDFT).^[44] If the dynamic response of the environment is neglected,^[45] the approximations are known in the literature as neglect of dynamic response of the environment (NDRE) or uncoupled frozen density embedding [FDE(u)].^[46] The NDRE approximation is applicable in the case of local excitations and negligible absorption by the environment in the investigated spectral range, as shown comprehensively by Neugebauer.^[46] In such a case, the functional derivative of the embedding potential with respect to $\rho_A(\vec{r})$ contributes to the response kernel $f(\vec{r}, \vec{r}')$ defined in LR-TDDFT with Equation (6):^[45]

$$f^{\text{emb}}(\vec{r}, \vec{r}') = \frac{\delta^2 E_{\text{xc}}^{\text{nad}}[\rho_A, \rho_B](\vec{r})}{\delta \rho_A(\vec{r}) \delta \rho_A(\vec{r}')} + \frac{\delta^2 T_s^{\text{nad}}[\rho_A, \rho_B](\vec{r})}{\delta \rho_A(\vec{r}) \delta \rho_A(\vec{r}')} \quad (6)$$

If the same approximations are used for $T_s^{\text{nad}}[\rho_A, \rho_B]$ and $E_{\text{xc}}^{\text{nad}}[\rho_A, \rho_B]$ in expressions for the energy, embedding potential, and response kernel, the excitation energies are also self-consistent with other properties of the embedded system.

2.2. Generation of the Averaged Charge Density of the Solvent Preserving Self-Consistency between ρ_A and $\langle \rho_B(\vec{r}) \rangle$

In typical FDET-based numerical simulations, the frozen density $\rho_B(\vec{r})$ is obtained from some approximate methods of quantum chemistry applied to the environment in a given structure. The key feature of FDET is, however, that any density can be used in FDET as $\rho_B(\vec{r})$. The present work concerns applications of FDET in which $\rho_B(\vec{r})$ is the statistically averaged electron density of the solvent (denoted here with $\langle \rho_B(\vec{r}) \rangle$). The FDET equations given in the previous section remain the same, with $\rho_B(\vec{r})$ being replaced by $\langle \rho_B(\vec{r}) \rangle$ and the environment part of the external potential $v_B(\vec{r})$ being replaced by its average $\langle v_B(\vec{r}) \rangle$. Such use of an FDET equation was introduced in Ref. [22] and comprehensively benchmarked in Ref. [23] for modeling solvatochromism of absorption. $\langle \rho_B(\vec{r}) \rangle$ is a continuum nonuniform descriptor of the solvent. The specific solute–solvent interactions are reflected in $\langle \rho_B(\vec{r}) \rangle$ in a statistical manner. In principle, any method can be used to generate the average quantities $\langle \rho_B(\vec{r}) \rangle$. The most straightforward is to use explicit atomic-level simulation of the solvated system and average the required quantities. Such an approach has been applied to average the electrostatic potential generated by the solvent,^[47,48] which can be seen as an approximate FDET method in which the last two terms of the FDET embedding potential [Eq. (5)] are completely neglected. In the present work, we use another procedure to

obtain the average quantities $\langle \rho_B(\vec{r}) \rangle$ and $\langle v_B(\vec{r}) \rangle$, which have been previously applied.^[22,23] The procedure is based on classical statistical theory of liquids. In the first step, the 3D-RISM equations^[19] with Hirata–Kovalenko closure^[20] are used to obtain the site probabilities, that is, the probability of finding a particular atom in a given volume element, which is a function in R^3 . In the next step, $\langle \rho_B(\vec{r}) \rangle$ is obtained as a sum of contributions due to each type of atom in the system. The contribution of each atom is, in turn, obtained as the convolution of the site probability with a simple (spherically symmetric) model of electron density of the atom. The details of this procedure are given in Refs. [22,23]. Here, we underline that in the applied procedure, the 3D-RISM and FDET equations are coupled in a self-consistent manner. The 3D-RISM site probabilities depend on the net charges on atoms of the embedded species, that is, on $\rho_A(\vec{r})$, whereas the embedded density depends on $\langle \rho_B(\vec{r}) \rangle$.

2.3. Simulation of Solvatochromism in Absorption versus Emission

The formal framework for multilevel simulations based on coupled 3D-RISM and FDET equations and self-consistent ρ_A and $\langle \rho_B \rangle$ outlined in the previous sections and already applied for studies of solvatochromism in absorption can, in principle, be extended for emission in a straightforward manner. The case of emission involves, however, an additional complication concerning the numerics and/or specific properties of the chromophores and solvents.

Assuring proper coupling depends on a procedure to generate the average net atomic charges of the embedded chromophore in the excited state. The electron density in the excited state is usually more delocalized than in the ground state; therefore, the delocalization might make the numerical procedure prone to numerical instabilities as far as assuring self-consistency between ρ_A and $\langle \rho_B \rangle$ is concerned. In fact, some decomposition schemes (Mulliken charges for instance) led to numerical instabilities in FDET/3D-RISM studies of solvatochromism in absorption.^[22] The procedure based on multipole derived atomic charges was chosen, because of its numerical robustness.^[22] The second complication concerns the physicochemical properties of the chromophore, the effect of the environment on both the structure and the charge distribution of the chromophore in its excited state. We advocate the use of the FDET strategy using the average continuum nonhomogeneous descriptor of the solvent $\langle \rho_B(\vec{r}) \rangle$ only for structurally rigid chromophores, that is, where the statistical nature is mainly manifested by the solvent and not by the solute. Otherwise, the FDET/3D-RISM strategy assuring a complete self-consistency between ρ_A , $\langle \rho_B \rangle$, and the average geometry of the solvated chromophore in the excited state, might not be practical. In the present work, we therefore estimate the relative importance of these effects and propose additional approximations within the FDET/3D-RISM strategy to deal with the effect of the solvent on geometry and the charge distribution of the chromophore in its excited state in a simplified manner.

2.4. Generation of the Averaged Charge Density of the Solvent without Self-Consistency between $\rho_A(\vec{r})$ and $\langle \rho_B(\vec{r}) \rangle$

As indicated in Figure 1, the effect of $\langle \rho_B(\vec{r}) \rangle$ on the electron density $\langle \rho_B(\vec{r}) \rangle$ (and all resulting properties) of the embedded species is taken into account by the FDET embedding potential given in Equation (5). This functional depends on $\langle \rho_B(\vec{r}) \rangle$. Taking into account the opposite effect, changes in $\langle \rho_B(\vec{r}) \rangle$, due to changing the state of the embedded subsystem, arise from the appropriate change of position and magnitude of the net atomic charges used as the input quantities for 3D-RISM equations. It is tempting to avoid such self-consistent treatment of $\rho_A(\vec{r})$ and $\langle \rho_B(\vec{r}) \rangle$ and to obtain the 3D-RISM parameters without it by means of an appropriately chosen set of atomic charges of the embedded species. For instance, in the work using averaged electrostatic potential of the solvent it has been argued^[49] that the self-consistency condition can be dropped without noticeable deterioration of the results. Following this suggestion, we consider three simplified methods to model the effect of changes in $\rho_A(\vec{r})$ on $\langle \rho_B(\vec{r}) \rangle$ (see Figure 1). They differ in the method used to generate the atomic net charges and positions for the embedded species in a given electronic state, for use in the 3D-RISM calculations:

- 1) The net atomic charges of the embedded species are evaluated at the optimized geometry without taking into account the solvent.
- 2) The net atomic charges of the embedded species are evaluated at the geometry optimized in the gas phase. The effect of the solvent on distribution of charges in the embedded species is taken into account by means of the PCM model.
- 3) Both the net atomic charges and the geometry of the embedded species are obtained by using PCM representation of the solvent.

In contrast to the self-consistent variant of FDET/3D-RISM calculations, the net atomic charges of the embedded species, once calculated, are fixed in the procedure to solve 3D-RISM equations.

3. Results and Discussion

3.1. Average Charge Densities of the Solvents

For a given set of atomic net charges of the chromophore, the non-self-consistent charge densities are obtained from the 3D-RISM calculations as a sum of the average electron density $\langle \rho_B(\vec{r}) \rangle$ and average nuclear charge density. The first quantity is needed to express the last three terms in the FDET embedding potential given in Equation (5), whereas the second is used to express $\langle v_B(\vec{r}) \rangle$. These two charge densities have opposite signs and vary rapidly, therefore, only the sum (average net charge) is discussed in this section. The average net charge density is obtained by Equation (7):

$$\langle \rho_B^{\text{net}}(\vec{r}) \rangle = \sum_{\gamma} q_{\gamma}^{\text{v,net}} \rho_{\gamma}^{\text{v}} g_{\gamma}^{\text{uv}}(\vec{r}) \quad (7)$$

where $q_{\gamma}^{\text{v,net}}$ represents a net charge characterizing a given type of atom (γ called site in 3D-RISM terminology) of the solvent, ρ_{γ}^{v} is solvent site density, and $g_{\gamma}^{\text{uv}}(\vec{r})$ is the 3D solute–solvent site distribution function obtained from 3D-RISM. The plots of net charge solvent density of the ground and excited state of C153 in five different solvents are shown in Figure 2, organized in descending order of solvent polarity. All the presented plots were made by using ADFview software.^[50] In case of water and methanol, the positive charge is localized close to carbonyl group of C153, which corresponds to hydrogen atoms forming a hydrogen bond with the carbonyl oxygen atom.

The three areas of positive charge density (see Figure 2) close to the carbonyl oxygen atom correspond to the possible arrangements of the hydrogen bonds. The first shell represent the arrangement of positively charged group (H with $q_{\gamma}^{\text{v,net}}$ 0.4238 e) followed by a second shell of negatively charged group (O with $q_{\gamma}^{\text{v,net}}$ -0.8476 e). The net atomic charges for acetonitrile are: 0.269 e on CH₃, 0.129 e on C, and -0.398 e on N. Compared with the charge on the oxygen atom of water, the negative charge of the nitrogen atom in acetonitrile is smaller. The negatively charged domains are, thus, less pronounced. Acetonitrile, acetone, and diethyl ether are aprotic solvents. The positively charged domain of the net charge density lies, therefore, further from the carbonyl oxygen atom of the chromophore. The well-organized pattern of the contour map represents the highly organized structure of acetone and diethyl ether compared with those of strongly polar solvents (water, acetonitrile, and propanol). The structure of the first shell is clearly visible near the solute.

For water and acetone, the solvent appears to be more structured compared with other bulky solvents. Except in the case of methanol and the other two alcohols, the ground and excited state charge distributions for highly polar and apolar solvents are indistinguishable on the figures. For the alcohols, small differences can be observed (plots for ethanol and 2-propanol are shown in the Supporting Information). The positively charged domain is more prominent in the case of the excited state of embedded chromophore and extends on the right side of the carbonyl group. The net charge is more attractive in this region for the excited electronic state of the molecule compared with that in the ground state. In addition, for all three alcohols, a small region of positive charge is localized near the CF₃ group.

The features of the densities of the average net charge are reflected in the embedding potential. The embedding potential for water and cyclohexane (in the ground state of C153) are shown in Figure 3a,b (for other solvents see the Supporting Information). Notably, both cases feature a cavity in which the chromophore is localized. The Pauli repulsion (or quantum confinement effect) is reflected by the positive edge defining the shape of the cavity. Within the cavity, the embedding potential is qualitatively different in the two cases. It is practically constant for cyclohexane, whereas it varies noticeably in the

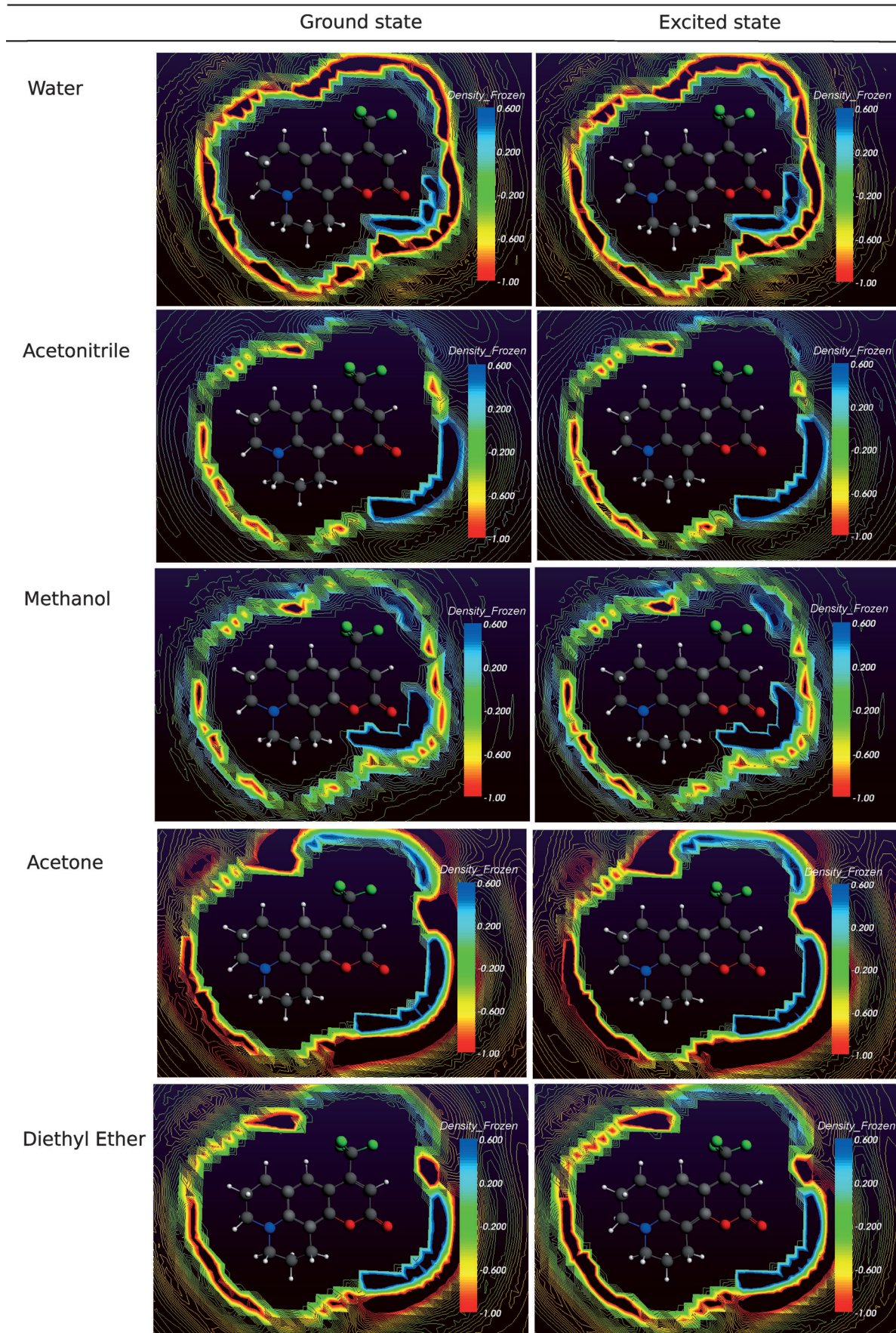


Figure 2. Density of the net average charge for the corresponding solvents in the ground- and excited-state of C153 (in atomic units). No map is shown for cyclohexane, because no structure would be visible for this apolar solvent with the color coding used here.

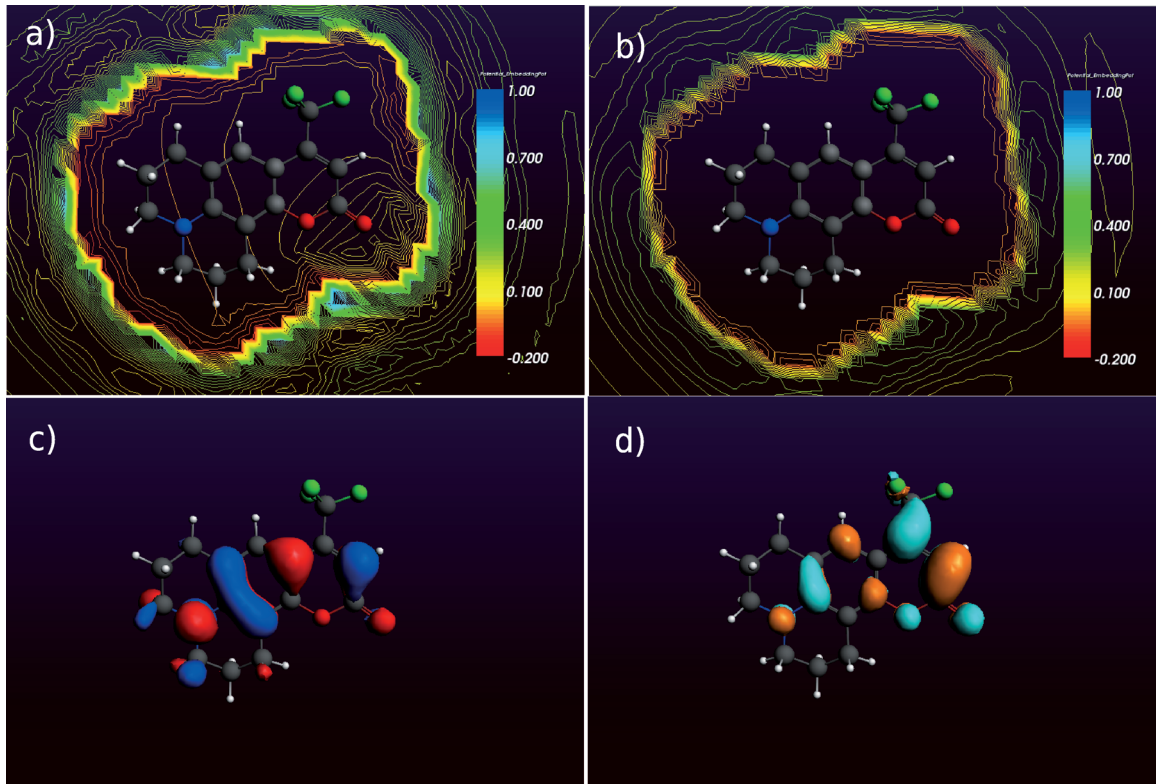


Figure 3. Embedding potential for the ground-state of C153 in a) water and b) cyclohexane. The lower panels show the frontier molecular orbitals of isolated C153: c) HOMO and d) LUMO.

case of water. It is the embedding potential within the cavity that determines the effect of the solvent on the orbital energies of the chromophore and, hence, the excitation energies. The molecular orbitals involved in electronic excitation of C153 are the highest occupied molecular orbital (HOMO; see Figure 3c) and the lowest unoccupied molecular (LUMO; see Figure 3d). The potentials shown in Figure 3 reflect clearly the difference in polarity of these solvents. For water, which is a highly polar protic solvent, the embedding potential is attractive close to the carbonyl group where the LUMO is localized on chromophore. The potential is repulsive on the opposite side of the chromophore. The zero line passes through the center of the molecule. These conditions lead to selective stabilization/destabilization of HOMO and LUMO. As a result, the HOMO–LUMO gap is reduced.

Interestingly, a more detailed look at the embedding potential shows some differences between the case of excited and ground states of the embedded chromophore (plots are given in the Supporting Information). The embedding potential is more repulsive from the center of the molecule to its left side. More orange lines (indicating repulsion) can be seen in this domain in the excited state. This observation correlates well with the measured strong redshifts of the $\pi \rightarrow \pi^*$ emission band for C153 molecule in polar solvents.

3.1.1. Solvatochromic Shifts

The FDET/3D-RISM solvatochromic shifts for absorption maxima calculated with different methods to evaluate non-

self-consistent net atomic charges of the embedded chromophore together with their experimental counterparts^[6] are given in Table 1. All other technical details of the calculations (the use of the SAOP exchange-correlation potential in particular) were the same as in our previously reported work.^[23] Table 1 clearly shows that taking into account the effect of the solvent on the atomic charges for the embedded chromophore is indispensable. The solvatochromic shifts calculated with Model 1 are up to 37% smaller than the experimental values. The shifts calculated with Model 2 and Model 3 are similar to the self-consistent FDET/3D-RISM results.

For modeling solvatochromism in emission, for which the effect of the solvent and excitation on the geometry of the chromophore cannot be neglected, we could not continue using the SAOP exchange–correlation potential, because the corresponding energy functional does not exist. Apart from the calculations reported in Table 1, all FDET/3D-RISM calculations reported in the present work were therefore, performed by using the B3LYP approximation for the exchange–correlation energy. Interestingly, the solvatochromic shifts in absorption obtained by using this functional, which are also provided in Table 1, agree even better with experiment than the SAOP results.

Previously reported solvatochromic shift in absorption^[23] were calculated by using STO-TZ2P (-0.29 eV in water and -0.24 eV in methanol) and augmented STO-TZ2P basis (-0.31 eV in water and -0.25 eV in methanol) and the same approximations for the density functionals in FDET. For corresponding shifts in rest of the solvents see Ref. [23]. The shifts

Table 1. FDET/3D-RISM and experimental solvatochromic shifts (in eV)^[a] of the $\pi \rightarrow \pi^*$ absorption band of coumarin 153. For the exchange-correlation potential generated at ρ_A , either SAOP or B3LYP approximation was used. The oscillatory strengths for the corresponding solvents are given in parentheses for Model 3.

| Solvent | ϵ | SAOP Model 1 | Model 2 | Model 3 | Self-consistent | B3LYP Model 3 | Experiment |
|-------------------|------------|-----------------|---------|---------|-----------------|------------------|---|
| H ₂ O | 78 | -0.17 | -0.23 | -0.24 | -0.27 | -0.29 (0.301) | -0.28 ^[b] |
| acetonitrile | 38 | -0.12 | -0.16 | -0.16 | -0.17 | -0.19 (0.343) | -0.20 ^[b] -0.20 ^[c] |
| methanol | 33 | -0.15 | -0.20 | -0.21 | -0.22 | -0.25 (0.329) | -0.23 ^[b] -0.24 ^[c] |
| ethanol | 25 | -0.14 | -0.18 | -0.19 | -0.20 | -0.23 (0.333) | -0.24 ^[c] |
| acetone | 21 | -0.12 | -0.17 | -0.18 | -0.20 | -0.21 (0.341) | -0.22 ^[c] |
| 1-propanol | 20 | -0.13 | -0.17 | -0.18 | -0.19 | -0.22 (0.335) | -0.23 ^[c] |
| 2-propanol | 20 | -0.13 | -0.17 | -0.18 | -0.19 | -0.22 (0.335) | -0.23 ^[c] |
| Et ₂ O | 4 | -0.09 | -0.12 | -0.12 | -0.14 | -0.14 (0.341) | -0.10 ^[c] |
| cyclohexane | 2 | 0.00 | 0.00 | 0.00 | 0.00 | 0.00 (0.348) | 0.00 ^[c] |

[a] The STO-DZP basis set was applied for all calculations. [b] Ref. [28]. [c] Ref. [6].

obtained in the present work (see Table 1, SAOP, Model 3) by using another basis set (STO-DZP) are close to those reported from our previous calculation for all the solvents. This proves the robustness of our method, which results from the variational principle on which FDET is based.

The same trend can be seen for all nine solvents of different polarities. The results obtained for absorption indicate clearly that at least Model 2 must be used for generation of non-self-consistent net atomic charges of the solvated chromophore for FDET/3D-RISM simulations of solvatochromic shifts in emission.

Only Models 2 and 3 are relevant for the study of solvatochromism in emission. Model 1 leads to the same average charge density of the solvent in the case of absorption and emission. Moreover, the numerical results obtained with Model 1 discussed in the previous sections show that taking into account the effect of the solvent on the net atomic charges of the embedded species is indispensable. The geometry of C153 in the first singlet excited state was optimized by using LR-TDDFT calculations. The partial charges fitted with electrostatic potential (ESP)^[51,52] were calculated by using configuration interaction singles (CIS)^[53] wavefunction. The solvatochromo-

mic shifts in emission are reported in Table 2. Models 2 and 3 lead to good agreement with experimental solvatochromic shifts in both protic and aprotic solvents. The results obtained by using Model 2 and Model 3 differ by only about 0.05–0.01 eV, indicating that the optimization of excited-state geometry of the chromophore in the PCM cavity (Model 3) is not crucial. Model 2 is, thus, sufficient to take into account the effect of the change of the state of the embedded species on the average charge density in the solvent in the FDET/3D-RISM evaluation of the solvatochromic shift.

All the calculations discussed so far use the nonuniform continuum representation of the whole solvent and only the chromophore is described at the quantum-mechanical level. Below, Model 3 is applied together with a different choice of embedded subsystem that includes not only the chromophore, but also one or two solvent molecules in the case of water and methanol. The results are collected in Table 3.

Table 3. FDET/3D-RISM solvatochromic shift (in eV)^[a] of the $\pi \rightarrow \pi^*$ emission band of coumarin 153 calculated using explicit solvent molecules in Model 3. For the exchange-correlation potential generated at ρ_A , B3LYP approximation was used.

| Solvent | Number of explicit solvent molecules (0) | (1) | (2) |
|------------------|---|-------|-------|
| H ₂ O | -0.49 | -0.44 | -0.47 |
| methanol | -0.43 | -0.44 | -0.44 |

[a] The STO-DZP basis set was applied for all calculations.

Table 2. FDET/3D-RISM and experimental solvatochromic shifts (in eV)^[a] of the $\pi \rightarrow \pi^*$ emission band of coumarin 153. For the exchange-correlation potential generated at ρ_A , the B3LYP approximation was used. The oscillatory strengths for the corresponding solvents are given in parentheses for Model 2 and Model 3.

| Solvent | ϵ | Model 2 | Model 3 | Experiment |
|-------------------|------------|---------------|---------------|---|
| H ₂ O | 78 | -0.54 (0.176) | -0.49 (0.232) | -0.46 ^[b] |
| acetonitrile | 38 | -0.39 (0.188) | -0.36 (0.249) | -0.38 ^[b] -0.42 ^[c] |
| methanol | 33 | -0.47 (0.180) | -0.43 (0.238) | -0.43 ^[b] -0.47 ^[c] |
| ethanol | 25 | -0.44 (0.180) | -0.40 (0.240) | -0.45 ^[c] |
| acetone | 21 | -0.44 (0.188) | -0.40 (0.247) | -0.38 ^[c] |
| 1-propanol | 20 | -0.42 (0.189) | -0.39 (0.242) | -0.43 ^[c] |
| 2-propanol | 20 | -0.42 (0.183) | -0.39 (0.241) | -0.41 ^[c] |
| Et ₂ O | 4 | -0.32 (0.189) | -0.32 (0.236) | -0.18 ^[c] |
| cyclohexane | 2 | 0.00 (0.195) | 0.00 (0.229) | 0.00 ^[c] |

[a] The STO-DZP basis set was applied for all calculations. [b] Ref. [28]. [c] Ref. [6].

In the optimized geometry of the embedded cluster, the explicitly treated solvent molecules form a bifurcated hydrogen bond with the carbonyl oxygen atom of chromophore. In the case of methanol, any choice of the size of the cluster representing the solvent explicitly leads to equivalent results (excitation energies are affected by 0.01 eV at most). In the case of water, the effect is also insignificant. The excitation energies obtained with none or two explicit water molecules agree within 0.02 eV. Interestingly, treating only one of the two tightly bound water molecules affects the excitation energy slightly more (0.05 eV), which indicates the need for a balanced treatment of the solvent molecules in the first solvation shell. Fluctuations of the position of the explicitly treated water molecule were neglected, whereas they were taken into account for the other tightly bound water molecules.

Table 4 collects the FDET/3D-RISM Stokes shifts. Calculated and experimental values are in reasonable agreement, although the discrepancies between the experiment and calcula-

Table 4. FDET/3D-RISM and experimental Stokes shifts (in eV)^[a] of the $\pi \rightarrow \pi^*$ transition in coumarin 153. For the exchange-correlation potential generated at ρ_A , the B3LYP approximation was used.

| Solvent | ϵ | Model 2 | Model 3 | Experiment |
|-------------------|------------|---------|---------|--|
| H ₂ O | 78 | 0.71 | 0.61 | 0.59 ^[b] |
| acetonitrile | 38 | 0.66 | 0.57 | 0.59, ^[b] 0.75 ^[c] |
| methanol | 33 | 0.69 | 0.59 | 0.60, ^[b] 0.75 ^[c] |
| ethanol | 25 | 0.67 | 0.58 | 0.74 ^[c] |
| acetone | 21 | 0.69 | 0.60 | 0.68 ^[c] |
| 1-propanol | 20 | 0.67 | 0.58 | 0.72 ^[c] |
| 2-propanol | 20 | 0.67 | 0.58 | 0.71 ^[c] |
| Et ₂ O | 4 | 0.63 | 0.58 | 0.60 ^[c] |
| cyclohexane | 2 | 0.46 | 0.47 | 0.52 ^[c] |

[a] The STO-DZP basis set was applied for all calculations. [b] Ref. [28].
[c] Ref. [6].

tions are slightly larger than the differences between the solvatochromic shifts in either emission or absorption. The Stokes shifts (calculated and experimental) vary significantly less than shifts in either absorption or emission if the polarity of the solvent changes. This indicates that the major factor determining the Stokes shifts in this chromophore is the change of the geometry of the chromophore upon excitation.

4. Conclusions

The nonuniform continuum model of the solvent used in FDET calculations of excitation energies, which was introduced previously for modeling solvatochromic shifts in absorption, was used to model solvatochromic shifts in emission. A simplified treatment of the coupling between the electron distribution in embedded species with statistically averaged charge distributions was introduced. The proposed methodology is suited for studies of the UV/Vis spectra of solvated rigid organic chromophores. The approach leads to numerical values of solvatochromic shifts in absorption and emission as well as the Stokes shifts, which compare well with experiment, and can be rationalized by means of a graphical feature of the FDET embedding potential evaluated at average charge density of the solvent. However, the FDET calculations with average solvent charge density cannot be applied to model shapes of inhomogeneously broadened bands, because the information about the solvent fluctuations is not contained in the average charge density of the solvent. These limitations are compensated for by the enormous computational savings compared with simulating band shapes. The latter type of simulation involves sampling a large number of solvent structures, whereas the methodology applied here involves only two calculations: for the embedded species with and without the environment. Finally, it is notable that the method used to generate the average charge density of the solvent is not limited to that used in the present work. Instead of using classical statistical-mechanical (3D-RISM) methods to obtain site probabilities, any other method could be used for this purpose. The averaged quantities obtained from the 3D-RISM equations are, in principle, equivalent to the ensemble average of the sufficiently long

atomistic simulation using the same pair-potentials as those used in the 3D-RISM equations.

Computational Details

The ground-state geometry of C153 was taken from our previous calculations, which was optimized in the KS-DFT framework by using the BP86^[54,55] exchange correlation functional. The excited-state geometry of the chromophore was optimized with TDDFT by using the B3LYP^[56–58] functional and polarized DFT orbital basis sets, TZVP.^[59,60] The solute charge distribution was calculated by fitting electrostatic potential to atomic charges (ESP) by using Merz-Sing-Kollman method.^[51,52] The excited-state charges were calculated by using the CIS^[53] wavefunction. GAUSSIAN 09^[61] software was used to evaluate net atomic charges and geometries of the embedded chromophore used subsequently in non-self-consistent FDET/3D-RISM calculations. To study solvatochromism in coumarin 153, solvent distribution was obtained from the 3D-RISM-KH^[62,63] scheme followed by FDET/TDDFT calculations to obtain excitation energies in the Amsterdam density functional software package (ADF).^[63] The cell size for the grid was chosen as $32 \times 32 \times 32 \text{ \AA}$ with $64 \times 64 \times 64$ grid points in the cell. The van der Waals parameters for solving the 3D-RISM-KH equation were taken from the OPLS force field for both solute–solute and solute–solvent interactions.^[64,65]

The effective embedding potential was evaluated for pairs of densities $\rho_A(\vec{r})$ and $\langle \rho_B(\vec{r}) \rangle$, using the local density approximation, for each of its nonelectrostatic components, the Thomas–Fermi expression for kinetic energy,^[66,67] the Dirac expression for the exchange energy,^[68] and Vosko–Wilk–Nusair expression for the correlation energy.^[69,70] The electrostatic component was obtained by using the monomer expansion of the 3D-RISM potential using all the center of the 3D-RISM grid. The exchange-correlation component of total effective potential, $(\delta E_{xc}[\rho_A]) / (\delta \rho_A)$ was approximated by using SAOP.^[71,72] Shifts are also calculated with the B3LYP exchange-correlation functional. In all the calculations, the Slater type atomic STO-DZP basis set was used to expand orbitals on the chromophore, which includes atomic centers localized only on the chromophore.

Acknowledgements

This research was supported by the Swiss National Science Foundation (200021_152775) and COST (European Cooperation in Science and Technology) Action CM1002.

Keywords: density functional calculations • molecular dynamics • molecular modeling • solvatochromism • UV/Vis spectroscopy

- [1] X. X. Zhang, M. Liang, N. P. Ernsting, M. Maroncelli, *J. Phys. Chem. B* **2013**, *117*, 4291–4304.
- [2] J. Sworakowski, J. Lipiński, Ł. Ziόłek, K. Palewska, S. Nespuřek, *J. Phys. Chem.* **1996**, *100*, 12288–12294.
- [3] S. Fleming, A. Mills, T. Tuttle, *Beilstein J. Org. Chem.* **2011**, *7*, 432–441.
- [4] P. O. Tuck, R. C. Mawhinney, M. Rappon, *Phys. Chem. Chem. Phys.* **2009**, *11*, 4471–4480.
- [5] C. Reichardt, *Chem. Rev.* **1994**, *94*, 2319–2358.
- [6] M. L. Horng, J. A. Gardecki, A. Papazyan, M. Maroncelli, *J. Phys. Chem.* **1995**, *99*, 17311–17337.
- [7] C. J. Cramer, D. G. Truhlar, *Chem. Rev.* **1999**, *99*, 2161–2200.

- [8] M. Hidalgo, R. Rivelino, S. Canuto, *J. Chem. Theory Comput.* **2014**, *10*, 1554–1562.
- [9] J. Aqvist, A. Warshel, *Chem. Rev.* **1993**, *93*, 2523–2544.
- [10] J. Sauer, P. Ugliengo, E. Garrone, V. R. Sounders, *Chem. Rev.* **1994**, *94*, 2095–2160.
- [11] A. Gao, *Reviews in computational chemistry*, Vol. 7 (Eds.: K. B. Lipkowitz, D. B. Boyd), VCH, New York, **1996**, p. 119.
- [12] D. Bakowies, W. Thiel, *J. Phys. Chem.* **1996**, *100*, 10580–10594.
- [13] O. Engkvist, P. O. Åstrand, G. Karlström, *Chem. Rev.* **2000**, *100*, 4087–4108.
- [14] J. Tomasi, B. Mennucci, R. Cammi, *Chem. Rev.* **2005**, *105*, 2999–3094.
- [15] A. Klamt, *J. Phys. Chem.* **1995**, *99*, 2224–2235.
- [16] A. Klamt, G. Schuurmann, *J. Chem. Soc. Perkin Trans. 2* **1993**, 799–805.
- [17] D. Chandler, H. C. Andersen, *J. Chem. Phys.* **1972**, *57*, 1930–1937.
- [18] S. Ten-no, F. Hirata, S. Kato, *Chem. Phys. Lett.* **1993**, *214*, 391–396.
- [19] A. Kovalenko, *Molecular Theory of Solvation in Understanding Chemical Reactivity*, Vol. 24, (Ed.: F. Hirata), Kluwer Academic, Dordrecht, **2003**, pp. 169–275.
- [20] A. Kovalenko, F. Hirata, *J. Chem. Phys.* **2000**, *112*, 10391–10402.
- [21] W. Kohn, L. J. Sham, *Phys. Rev.* **1965**, *140*, A1133–A1138.
- [22] J. W. Kaminski, S. Gusalov, T. A. Wesolowski, A. Kovalenko, *J. Phys. Chem. A* **2010**, *114*, 6082–6096.
- [23] X. Zhou, J. W. Kaminski, T. A. Wesolowski, *Phys. Chem. Chem. Phys.* **2011**, *13*, 10565–10576.
- [24] T. A. Wesolowski, J. Weber, *Chem. Phys. Lett.* **1996**, *248*, 71–76.
- [25] M. Humbert-Droz, X. Zhou, S. V. Shedge, T. A. Wesolowski, *Theor. Chem. Acc.* **2013**, *133*, 1405.
- [26] C. Daday, C. König, O. Valsson, J. Neugebauer, C. Filippi, *Chem. Phys. Lett.* **1996**, *248*, 71–76.
- [27] M. Zbiri, M. Atanasov, C. Daul, J. M. Garcia-Lastra, T. A. Wesolowski, *Chem. Phys. Lett.* **2004**, *397*, 441–446.
- [28] P. Hazra, D. Chakrabarty, N. Sarkar, *Chem. Phys. Lett.* **2003**, *371*, 553–562.
- [29] T. A. Wesolowski, A. Warshel, *J. Phys. Chem.* **1993**, *97*, 8050–8053.
- [30] T. A. Wesolowski, *Computational Chemistry: Reviews of Current Trends*, Vol. 10 (Ed.: J. Leszczynski), World Scientific, Singapore, **2006**, pp. 1–82.
- [31] T. A. Wesolowski, *Phys. Rev. A* **2008**, *77*, 012504.
- [32] K. Pernal, T. A. Wesolowski, *Int. J. Quantum Chem.* **2009**, *109*, 2520–2525.
- [33] P. Hohenberg, W. Kohn, *Phys. Rev. B* **1964**, *136*, B864–B871.
- [34] M. Levy, *Proc. Natl. Acad. Sci. USA* **1979**, *76*, 6062–6065.
- [35] M. Levy, *Phys. Rev. A* **1982**, *26*, 1200–1208.
- [36] F. Shimojo, R. K. Kalia, A. Nakano, P. Vashishta, *Comput. Phys. Commun.* **2005**, *167*, 151–164.
- [37] O. Roncero, M. P. de Lara-Castells, P. Villarreal, F. Flores, J. Ortega, M. Paniagua, A. Aguado, *J. Chem. Phys.* **2008**, *129*, 184104.
- [38] M. Hodak, W. Lu, J. Bernholc, *J. Chem. Phys.* **2008**, *128*, 014101.
- [39] D. Lahav, T. Kluner, *J. Phys. Condens. Matter* **2007**, *19*, 226001.
- [40] D. G. Jason, A. Nandini, R. M. Frederick, F. M. Thomas III, *J. Chem. Phys.* **2010**, *133*, 084103.
- [41] A. S. P. Gomes, C. R. Jacob, L. Visscher, *Phys. Chem. Chem. Phys.* **2008**, *10*, 5353–5362.
- [42] M. Pavanello, *J. Chem. Phys.* **2013**, *138*, 204118.
- [43] N. Govind, Y. A. Wang, A. J. R. da Silva, E. A. Carter, *Chem. Phys. Lett.* **1998**, *295*, 129–134.
- [44] M. E. Casida, *Time-dependent density-functional response theory for molecules in Recent Advances in Density-Functional Methods* (Ed.: D. P. Chong), World Scientific, Singapore, **1995**, pp. 155.
- [45] T. A. Wesolowski, *J. Am. Chem. Soc.* **2004**, *126*, 11444–11445.
- [46] J. Neugebauer, *J. Chem. Phys.* **2007**, *126*, 134116.
- [47] K. Coutinho, H. C. Georg, T. L. Fonseca, V. Ludwig, S. Canuto, *Chem. Phys. Lett.* **2007**, *437*, 148–152.
- [48] I. F. Galván, M. L. Sánchez, M. E. Martín, F. J. O. del Valle, M. A. Aguilar, *Comput. Phys. Commun.* **2003**, *155*, 244–259.
- [49] H. C. Georg, K. Coutinho, S. Canuto, *J. Chem. Phys.* **2007**, *126*, 034507.
- [50] GUI 2013 SCM, Amsterdam, The Netherlands, **2013** <http://www.scm.com>.
- [51] U. C. Singh, P. A. Kollman, *J. Comput. Chem.* **1984**, *5*, 129–145.
- [52] B. H. Besler, K. M. Merz, P. A. Kollman, *J. Comput. Chem.* **1990**, *11*, 431–439.
- [53] J. B. Foresman, M. Head-Gordon, J. A. Pople, M. J. Frisch, *J. Phys. Chem.* **1992**, *96*, 135–149.
- [54] A. D. Becke, *Phys. Rev. A* **1988**, *38*, 3098–3100.
- [55] J. P. Perdew, *Phys. Rev. B* **1986**, *33*, 8822–8824.
- [56] A. D. Becke, *J. Chem. Phys.* **1993**, *98*, 5648–5652.
- [57] C. Lee, W. Yang, R. G. Parr, *Phys. Rev. B* **1988**, *37*, 785–789.
- [58] B. Miehlich, A. Savin, H. Stoll, H. Preuss, *Chem. Phys. Lett.* **1989**, *157*, 200–206.
- [59] A. Schäfer, H. Horn, R. Ahlrichs, *J. Chem. Phys.* **1992**, *97*, 2571–2577.
- [60] A. Schäfer, C. Huber, R. Ahlrichs, *J. Chem. Phys.* **1994**, *100*, 5829–5835.
- [61] Gaussian 09 (Revision D.01), M. J. Frisch, G. W. Trucks, H. B. Schlegel, G. E. Scuseria, M. A. Robb, J. R. Cheeseman, G. Scalmani, V. Barone, B. Mennucci, G. A. Petersson, H. Nakatsuji, M. Caricato, X. Li, H. P. Hratchian, A. F. Izmaylov, J. Bloino, G. Zheng, J. L. Sonnenberg, M. Hada, M. Ehara, K. Toyota, R. Fukuda, J. Hasegawa, M. Ishida, T. Nakajima, Y. Honda, O. Kitao, H. Nakai, T. Vreven, Montgomery, Jr., J. A., J. E. Peralta, F. Ogliaro, M. Bearpark, J. J. Heyd, E. Brothers, K. N. Kudin, V. N. Staroverov, R. Kobayashi, J. Normand, K. Raghavachari, A. Rendell, J. C. Burant, S. S. Iyengar, J. Tomasi, M. Cossi, N. Rega, J. M. Millam, M. Klene, J. E. Knox, J. B. Cross, V. Bakken, C. Adamo, J. Jaramillo, R. Gomperts, R. E. Stratmann, O. Yazyev, A. J. Austin, R. Cammi, C. Pomelli, J. W. Ochterski, R. L. Martin, K. Morokuma, V. G. Zakrzewski, G. A. Voth, P. Salvador, J. J. Dannenberg, S. Dapprich, A. D. Daniels, Á. Farkas, J. B. Foresman, J. V. Ortiz, J. Cioslowski, D. J. Fox, Inc. Wallington CT, **2009**.
- [62] S. Gusalov, T. Ziegler, A. Kovalenko, *J. Phys. Chem. A* **2006**, *110*, 6083–6090.
- [63] ADF2013.01, SCM, Theoretical Chemistry, Vrije Universiteit, Amsterdam, The Netherlands, <http://www.scm.com>, **2013**.
- [64] W. L. Jorgensen, J. D. Madura, C. J. Swenson, *J. Am. Chem. Soc.* **1984**, *106*, 6638–6646.
- [65] W. L. Jorgensen, D. S. Maxwell, J. Tirado-Rives, *J. Am. Chem. Soc.* **1996**, *118*, 11225–11236.
- [66] L. H. Thomas, *Math. Proc. Cambridge Philos. Soc.* **1927**, *23*, 542–548.
- [67] E. Fermi, *Z. Phys.* **1928**, *48*, 73–79.
- [68] P. A. M. Dirac, *Proc. Cambridge Philos. Soc.* **1930**, *26*, 376–385.
- [69] D. M. Ceperley, B. J. Alder, *Phys. Rev. Lett.* **1980**, *45*, 566–569.
- [70] S. H. Vosko, L. Wilk, M. Nusair, *Can. J. Phys.* **1980**, *58*, 1200–1211.
- [71] O. V. Gritsenko, P. R. T. Schipper, E. J. Baerends, *Chem. Phys. Lett.* **1999**, *302*, 199–207.
- [72] P. R. T. Schipper, O. V. Gritsenko, S. J. A. van Gisbergen, E. J. Baerends, *J. Chem. Phys.* **2000**, *112*, 1344–1352.

Received: May 20, 2014

Revised: July 9, 2014

Published online on August 29, 2014